OPEN ACCESS
JOURNAL OF ADVANCED DIELECTRICS
Vol. 11, No. 5 (2021) 2160009 (11 pages)

DOI: 10.1142/S2010135X21600092

Numerical investigation of the effects of partial metallization at the pore surface on the effective properties of a porous piezoceramic composite

Andrey Nasedkin*,‡ and Mohamed Elsayed Nassar*,†
*Institute of Mathematics, Mechanics & Computer Science
Southern Federal University
Miltchakova Str., 8a, Rostov-on-Don 344090, Russia
†Department of Physics and Engineering Mathematics
Faculty of Electronic Engineering
Menoufia University, 32952 Menouf, Egypt
‡avnasedkin@sfedu.ru

Received 14 April 2021; Accepted 4 June 2021; Published 25 August 2021

This paper presents a numerical homogenization analysis of a porous piezoelectric composite with a partially metalized pore surface. The metal layers can be added to the pore surfaces to improve the mechanical and electromechanical properties of ordinary porous piezocomposites. Physically, constructing that composite with completely metalized pore surfaces is a challenging process, and imperfect metallization is more expected. Here, we investigate the effects of possible incomplete metallization of pore surfaces on the composite's equivalent properties. We applied the effective moduli theory, which was developed for the piezoelectric medium based on the Hill–Mandel principle, and the finite element method to compute the effective moduli of the considered composites. Using specific algorithms and programs in the ANSYS APDL programming language, we constructed the representative unit cell element models and performed various computational experiments. Due to the presence of metal inclusion, we found that the dielectric and piezoelectric properties of the considered composites differ dramatically from the corresponding properties of the ordinary porous piezocomposites. The results of this work showed that piezocomposites with partially metallized pore surfaces can have a higher anisotropy, compared to the pure piezoceramic matrix, due to the defects in metal coatings.

Keywords: Piezoelectricity; piezoelectric composites; piezoelectric ceramic-metal composite; partial metalization; effective properties; finite element analysis.

1. Introduction

Owing to the unique electromechanical coupling properties of the piezoelectric materials, they have potential utility in many applications: particularly in the medical applications,[1,2] aerospace industries,[3] smart material systems,[4] microelectromechanical systems (MEMS),[5] and structural health monitoring (SHM).[6] Piezoelectric ceramics are the most frequently used piezoelectric materials because of their outstanding piezoelectric properties. Moreover, by incorporating a controlled porosity into the piezoelectric material, the efficiency of piezoelectric ultrasonic devices can be improved.[7–9] The porous piezocomposites are distinguished by greater piezoelectric voltage moduli ($g_{i\alpha}$), lower acoustic impedance (Z_a), and higher hydrostatic figure of merit (HFOM).[10–12] However, piezoceramics and, therefore, porous piezoceramic composites are fragile materials, and this imposes restrictions on their use.[13,14] The poor mechanical properties of the porous piezocomposites may lead to mechanical damage, dielectric breakdown, and low reliability.[15–17]

The incorporation of the metal particles into the piezoelectric matrix significantly improves its mechanical properties, especially the fracture toughness.[18–20] To enhance the mechanical properties of piezoelectric ceramics, a metal-core piezoelectric ceramic fiber/aluminum composite was formed using the interphase forming/bonding process.[21–23] In these works, the piezoelectric ceramic is strengthened by embedding it in an aluminum matrix. To improve the mechanical, electrical, and functional properties of porous piezoceramic composites, Rybyanets *et al.*[24,25] developed a novel approach for fabricating the piezocomposites by introducing various forms of polymeric micro granules, which are filled or coated with metal-containing micro- or nanoparticles, into the ceramic matrix during the manufacturing process. In this way, they created a metal layer from these micro- or nanoparticles on the pore surface. In our previously published work,[26] we considered the effects of polarization inhomogeneity on the effective material properties of that piezocomposite. Compared with the effective properties of ordinary porous piezocomposites, we found a dramatic shift in dielectric permittivity and some piezoelectric properties of the composite. To only investigate the effects of adding the metal layer on the dielectric and electromechanical coupling

properties, we assumed that the metal layer deposited on the pore surface has negligible thickness. Here, the system (piezocomposite) with a metalized pore surface is referred to (SMPS).

The SMPS is a three-phase composite with a closed porosity and, accordingly, with a closed metallization structure, i.e., 3–0–0 composite according to Newnham's definition for composites connectivity.[27] Due to the structural complexity of the SMPS, we implemented the numerical finite element analysis to determine its effective properties. Our approach involves computer modeling of the representative volume element (RVE) model, using the finite element analysis and the effective moduli method to obtain the macro-properties of composite over the RVE. This technique allows the internal structure of the porous composite to be considered, including the type of connectivity, pore sizes, and local effects such as the polarization field inhomogeneity.[26,28,29] We implemented a simple RVE consisting of a cube of piezoceramics, which contains a vacuum pore at its center and a metal layer at the interface between the piezoelectric and vacuum phases. Physically, constructing the piezocomposite (SMPS) with a completely metalized pore surface (SCMPS) is difficult; therefore, in this work, depending on our previous research,[26,30] we explore the influence of the incomplete metalization on the effective moduli of the SMPS. Consequently, we studied different cases for the system with a partially metalized pore surface (SPMPS). From the results of our computer investigations, we observed a major impact of the internal configuration of the RVE on the effective moduli and the crystal symmetry of the piezocomposite under consideration.

2. Mathematical Model and Methodology

2.1. *Representative volume element (RVE)*

The representative unit cell element or the representative volume Ω is a cube of piezoceramic matrix Ω^m, whose edge length equals L and contains a cubic compound pore Ω^c of edge length $B = L\sqrt[3]{v_c}$, where $v_c = |\Omega^c|/|\Omega|$ is the porosity volume fraction. The compound cubic pore Ω^c consists of a vacuum pore Ω^p besides the metal layer Ω^e coating some or all pore sides, i.e., $\Omega = \Omega^m \cup \Omega^c$ and $\Omega^c = \Omega^e \cup \Omega^p$.

As noted earlier,[26,30] when modeling a composite with a piezoceramic matrix, pores, and metal layers at the pore boundaries in ANSYS finite element package, it is sufficient to use piezoelectric elements (for example, SOLID227 in Fig. 1) for all three phases with the corresponding material

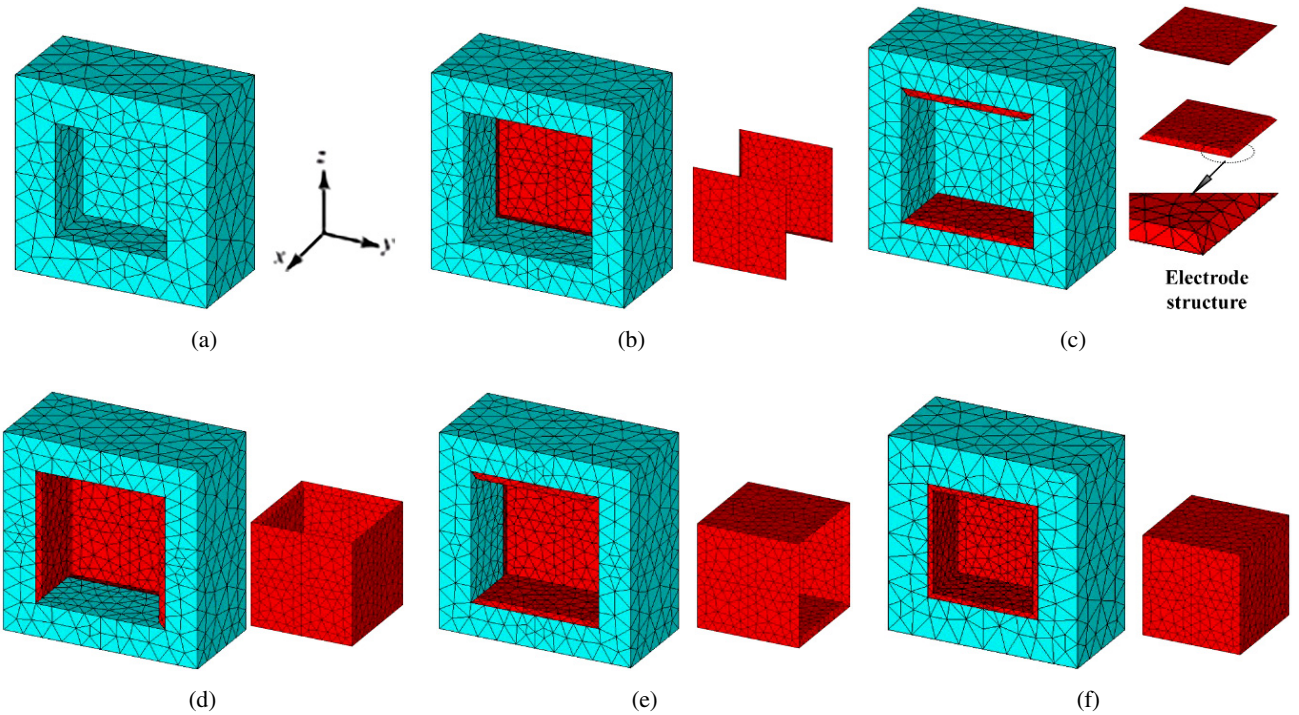

Fig. 1. (Color online) The half of the RVEs for composites without the vacuum pore: (a) OPS — ordinary porous system, (b) SPMPS2X — the system with a partially metalized pore surface, when two metalized pore sides are normal to the x-axis, (c) SPMPS2Z — the system with a partially metalized pore surface, whose metalized pore sides are normal to the z-axis, (d) SPMPS2X2Y — the system with a paritally metalized pore surface with two metalized pore sides normal to the x-axis and two metalized pore sides normal to the y-axis, (e) SPMPS2X2Z — the system with a partially metalized pore surface with two metalized pore sides normal to x-axis and two metalized pore sides normal to z-axis, and (f) SCMPS — the system with a completely metalized pore surface, at $v_c = 0.2$. The metal layer Ω^e on the pore surface is presented for each case using red elements.

properties, which have extreme values (very small or very large) for pores and metal interface layers.

For our new RVE with incomplete metallization of pore boundaries, it makes sense to discuss in more detail the features of modeling thin metal layers, for which the most important parameter is the area of the metal-piezoceramic contact surface. Unfortunately, there are no piezoelectric or dielectric shell elements in ANSYS to represent the metalized pore sides/electrodes. Therefore, we implemented tetrahedral SOLID227 elements with a small size to model the metal sides of the pore. Each metal layer (electrode) is designed as a 3D-trapezoid with a very thin thickness H, e.g., $H = B/20$. According to this design, only the greater square side of the electrode is connected to the piezoceramic matrix. The electrode design is clearly depicted in Fig. 1(c). The metal layer coating the vacuum pore is filled with a piezoelectric material with minimal elastic stiffness and piezoelectric moduli and very high dielectric permittivity moduli. The minimal elastic properties and the 3D-trapezoidal design of the metal layer simulate its actual negligible thickness. Due to the proposed design and material properties of the metal layer, the effective properties of the SMPS are independent of the metal coating's thickness (H).[30]

The vacuum pore is modeled as a piezoelectric material with negligible piezomoduli and elastic stiffness moduli and with dielectric permittivity of vacuum.

The SCMPS models the system with an optimally metalized pore surface; while the ordinary porous system (OPS) represents the ordinary porous piezocomposite without a metal layer, i.e., $\Omega^c = \Omega^p$. Figure 1 introduces the different cases of the RVEs understudy. The abbreviations denoting different cases of the SPMPS are shown in Fig. 1, accompanied by the metal layer's construction. For example, the abbreviation SPMPS2X2Z, in Fig. 1(e), signifies the SPMPS, which contains two metalized pore faces perpendicular to x-axis, and two metalized pore faces perpendicular to z-axis.

To construct the finite element model, we implemented 10-node 40-degrees of freedom tetrahedral SOLID227 elements. We utilized a free mesh with the ability to control the element size. The element size can be altered by controlling the maximum tolerable edge length. When restricting the maximum element edge length to $L/8$ ($L/8$ for the OPS and SCMPS and $L/10$ for the systems with partly metalized pore surface) for the piezoelectric and vacuum elements (Ω^m and Ω^p) and $2H$ for the metal layer elements (Ω^e), we got results with reasonable accuracy. In Fig. 1, the elements representing the piezoelectric matrix and the metal layer are plotted respectively in sky blue and red colors.

2.2. *Governing equations*

For quasi-static homogenization problems, the elastic and electric fields can be expressed using the simplified linear elasticity equations and Maxwell's equations as follows:

$$\mathbf{S} = \mathbf{L}(\nabla)\cdot\mathbf{u}, \quad \mathbf{E} = -\nabla\phi, \tag{1}$$

$$\mathbf{L}^*(\nabla) = \begin{bmatrix} \partial_1 & 0 & 0 & 0 & \partial_3 & \partial_2 \\ 0 & \partial_2 & 0 & \partial_3 & 0 & \partial_1 \\ 0 & 0 & \partial_3 & \partial_2 & \partial_1 & 0 \end{bmatrix}, \quad \nabla = \begin{Bmatrix} \partial_1 \\ \partial_2 \\ \partial_3 \end{Bmatrix}.$$

The quasi-electrostatic homogenization problem also involves the following equilibrium equations neglecting the body forces and the free charges

$$\mathbf{L}^*(\nabla)\cdot\mathbf{T} = 0, \quad \nabla\cdot\mathbf{D} = 0 \quad \mathbf{x}\in\Omega, \tag{2}$$

where $\mathbf{S} = \{s_{11}, s_{22}, s_{33}, 2s_{23}, 2s_{13}, 2s_{12}\}$ and $\mathbf{T} = \{\sigma_{11}, \sigma_{22}, \sigma_{33}, \sigma_{23}, \sigma_{13}, \sigma_{12}\}$ are, respectively, the arrays of the strains s_{ij} and of the stresses σ_{ij} in Viogt's matrix notation; $\mathbf{E}$, $\mathbf{D}$, ϕ, and $\mathbf{u}$ are the electric field vector, electric flux density vector, electric potential, and mechanical displacement vector, respectively; $\mathbf{L}$ is a matrix operator; ∇ is the gradient operator relative to the position vector $\mathbf{x}$, which can be expressed as $\mathbf{x} = \{x, y, z\} = \{x_1, x_2, x_3\}$. The constitutive equations of this system considering the linear piezoelectric theory can be written as follows:

$$\boldsymbol{\Sigma} = \boldsymbol{\Pi}\cdot\mathbf{Z}, \quad \boldsymbol{\Pi} = \begin{bmatrix} \mathbf{c}^E & -\mathbf{e}^* \\ \mathbf{e} & \boldsymbol{\varepsilon}^S \end{bmatrix}, \quad \boldsymbol{\Sigma} = \begin{Bmatrix} \mathbf{T} \\ \mathbf{D} \end{Bmatrix}, \quad \mathbf{Z} = \begin{Bmatrix} \mathbf{S} \\ \mathbf{E} \end{Bmatrix}. \tag{3}$$

Here, $\mathbf{c}^E$ is the 6×6 matrix of short-circuit elastic stiffness moduli; $\mathbf{e}$ is the 3×6 matrix of piezoelectric stress coefficients; $\boldsymbol{\varepsilon}^S$ is the 3×3 matrix of the clamped dielectric permittivity moduli; $(\ldots)^*$ is the matrix transpose operation; and $(\ldots)\cdot(\ldots)$ is the scalar product operation of matrices or vectors.

The boundary conditions can be generally represented by the following equation:

$$\mathbf{u} = \mathbf{L}^*(\mathbf{x})\cdot\mathbf{S}_0, \quad \phi = -\mathbf{x}\cdot\mathbf{E}_0, \quad \mathbf{x}\in\Gamma, \tag{4}$$

where $\Gamma = \partial\Omega$ is the external surface of the representative volume Ω; $\mathbf{S}_0$ and $\mathbf{E}_0$ are specific strain and electric field vectors, respectively, applied on the boundary Γ in a manner consistent with the concept of the theory of effective moduli.[30–32]

At the interface boundaries Γ^i of any two adjacent phases I and II (Ω^m, Ω^e, or Ω^p) of the composite, the full contact continuity conditions are met; consequently, we have[26,30]

$$\mathbf{u}^I = \mathbf{u}^{II}, \quad \mathbf{L}^*(\mathbf{n})\cdot\mathbf{T}^I = \mathbf{L}^*(\mathbf{n})\cdot\mathbf{T}^{II}, \quad \mathbf{x}\in\Gamma^i, \tag{5}$$

$$\phi^I = \phi^{II}, \quad \mathbf{n}\cdot\mathbf{D}^I = \mathbf{n}\cdot\mathbf{D}^{II}, \quad \mathbf{x}\in\Gamma^i, \tag{6}$$

where $\mathbf{n}$ is the unit normal vector to the boundary Γ^i.

2.3. *Effective moduli determination*

We considered the piezoelectric material PZT-5H with the properties: $c^E_{11} = 12.6\cdot 10^{10}$, $c^E_{12} = 7.95\cdot 10^{10}$, c^E_{13}

$= 8.41 \cdot 10^{10}$, $c_{33}^E = 11.7 \cdot 10^{10}$, $c_{44}^E = 2.3 \cdot 10^{10}$ (N/m^2), $e_{31} = -6.5$, $e_{33} = 23.3$, $e_{15} = 17.0$ (C/m^2), $\varepsilon_{11}^S = 1700\varepsilon_0$, $\varepsilon_{33}^S = 1470\varepsilon_0$, where $\varepsilon_0 = 8.85 \cdot 10^{-12}$ (F/m) is the vacuum dielectric permittivity. For the vacuum pore Ω^p the elastic, piezoelectric, and dielectric permittivity moduli are modeled, respectively, as $(c_{\alpha\beta}^E)^p = \kappa c_{\alpha\beta}^E$, $(e_{i\alpha})^p = \kappa$ (C/m^2) and $(\varepsilon_{11}^S)^p = \varepsilon_0$, where $\kappa = 10^{-10}$. For the metal layer Ω^e, we considered the elastic, piezoelectric, and dielectric permittivity moduli as follows: $(c_{\alpha\beta}^E)^e = \kappa c_{\alpha\beta}^E$, $(e_{i\alpha})^e = \kappa$ (C/m^2), $(\varepsilon_{ii}^S)^e = \mu\varepsilon_0$, where $\mu = 10^{12}$, $\alpha, \beta = 1, 2, \ldots, 6$, and $i = 1, 2, 3$.

To clarify the effective moduli of the SPMPS, we considered the most general electroelastic properties, which are 81 parameters. We assumed an asymmetric stiffness matrix (36 elastic constants), different values for direct and converse piezoelectric constants (36 piezomoduli), and nine permittivity constants. The macro properties obtained using analytical or numerical homogenization techniques must satisfy the Hill–Mandel principle.[33] This principle states that in the RVE, under the same external influences (4), the averaged potential energy $\langle U \rangle$ in a composite medium is identical to the potential energy U_0 in an equivalent homogeneous medium with effective moduli, which must be determined based on this condition.

The constitutive equations (3) for homogeneous effective medium can be written briefly in one equation

$$\boldsymbol{\Sigma}_0 = \boldsymbol{\Pi}^{\text{eff}} \cdot \mathbf{Z}_0, \tag{7}$$

where $\boldsymbol{\Sigma}_0 = \{\mathbf{T}_0, \mathbf{D}_0\}$ is the nine-component array of constant stresses and electrical displacement fields, $\mathbf{Z}_0 = \{\mathbf{S}_0, \mathbf{E}_0\}$ is the nine-component array of constant strains and electrical fields coinciding with the values $\mathbf{S}_0$ and $\mathbf{E}_0$ from (4). The detailed components of the arrays $\boldsymbol{\Sigma}_0$ and $\mathbf{Z}_0$, and the effective property matrix $\boldsymbol{\Pi}^{\text{eff}}$ are as follows:

$$\begin{aligned}
\boldsymbol{\Sigma}_0 &= \{\Sigma_{01}, \Sigma_{02}, \Sigma_{03}, \Sigma_{04}, \Sigma_{05}, \Sigma_{06}, \Sigma_{07}, \Sigma_{08}, \Sigma_{09}\} \\
&= \{T_{01}, T_{02}, T_{03}, T_{04}, T_{05}, T_{06}, D_{01}, D_{02}, D_{03}\}, \\
\mathbf{Z}_0 &= \{Z_{01}, Z_{02}, Z_{03}, Z_{04}, Z_{05}, Z_{06}, Z_{07}, Z_{08}, Z_{09}\} \\
&= \{s_{01}, s_{02}, s_{03}, s_{04}, s_{05}, s_{06}, E_{01}, E_{02}, E_{03}\},
\end{aligned}$$

$$\boldsymbol{\Pi}^{\text{eff}} = \left(\begin{array}{cccccc|ccc}
c_{11}^{E\,\text{eff}} & c_{12}^{E\,\text{eff}} & c_{13}^{E\,\text{eff}} & c_{14}^{E\,\text{eff}} & c_{15}^{E\,\text{eff}} & c_{16}^{E\,\text{eff}} & -e_{11}^{c\,\text{eff}} & -e_{21}^{c\,\text{eff}} & -e_{31}^{c\,\text{eff}} \\
c_{21}^{E\,\text{eff}} & c_{22}^{E\,\text{eff}} & c_{23}^{E\,\text{eff}} & c_{24}^{E\,\text{eff}} & c_{25}^{E\,\text{eff}} & c_{26}^{E\,\text{eff}} & -e_{12}^{c\,\text{eff}} & -e_{22}^{c\,\text{eff}} & -e_{32}^{c\,\text{eff}} \\
c_{31}^{E\,\text{eff}} & c_{32}^{E\,\text{eff}} & c_{33}^{E\,\text{eff}} & c_{34}^{E\,\text{eff}} & c_{35}^{E\,\text{eff}} & c_{36}^{E\,\text{eff}} & -e_{13}^{c\,\text{eff}} & -e_{23}^{c\,\text{eff}} & -e_{33}^{c\,\text{eff}} \\
c_{41}^{E\,\text{eff}} & c_{42}^{E\,\text{eff}} & c_{43}^{E\,\text{eff}} & c_{44}^{E\,\text{eff}} & c_{45}^{E\,\text{eff}} & c_{46}^{E\,\text{eff}} & -e_{14}^{c\,\text{eff}} & -e_{24}^{c\,\text{eff}} & -e_{34}^{c\,\text{eff}} \\
c_{51}^{E\,\text{eff}} & c_{52}^{E\,\text{eff}} & c_{53}^{E\,\text{eff}} & c_{54}^{E\,\text{eff}} & c_{55}^{E\,\text{eff}} & c_{56}^{E\,\text{eff}} & -e_{15}^{c\,\text{eff}} & -e_{25}^{c\,\text{eff}} & -e_{35}^{c\,\text{eff}} \\
c_{61}^{E\,\text{eff}} & c_{62}^{E\,\text{eff}} & c_{63}^{E\,\text{eff}} & c_{64}^{E\,\text{eff}} & c_{65}^{E\,\text{eff}} & c_{66}^{E\,\text{eff}} & -e_{16}^{c\,\text{eff}} & -e_{26}^{c\,\text{eff}} & -e_{36}^{c\,\text{eff}} \\
\hline
e_{11}^{d\,\text{eff}} & e_{12}^{d\,\text{eff}} & e_{13}^{d\,\text{eff}} & e_{14}^{d\,\text{eff}} & e_{15}^{d\,\text{eff}} & e_{16}^{d\,\text{eff}} & \varepsilon_{11}^{S\,\text{eff}} & \varepsilon_{12}^{S\,\text{eff}} & \varepsilon_{13}^{S\,\text{eff}} \\
e_{21}^{d\,\text{eff}} & e_{22}^{d\,\text{eff}} & e_{23}^{d\,\text{eff}} & e_{24}^{d\,\text{eff}} & e_{25}^{d\,\text{eff}} & e_{26}^{d\,\text{eff}} & \varepsilon_{21}^{S\,\text{eff}} & \varepsilon_{22}^{S\,\text{eff}} & \varepsilon_{23}^{S\,\text{eff}} \\
e_{31}^{d\,\text{eff}} & e_{32}^{d\,\text{eff}} & e_{33}^{d\,\text{eff}} & e_{34}^{d\,\text{eff}} & e_{35}^{d\,\text{eff}} & e_{36}^{d\,\text{eff}} & \varepsilon_{31}^{S\,\text{eff}} & \varepsilon_{32}^{S\,\text{eff}} & \varepsilon_{33}^{S\,\text{eff}}
\end{array}\right). \tag{8}$$

In accordance with the general theory of the effective moduli method for piezoelectric composites and Eqs. (1)–(8), the following equalities hold[30–34]:

$$2\langle U \rangle = \langle \boldsymbol{\Sigma} \cdot \mathbf{Z} \rangle = \langle \boldsymbol{\Sigma} \rangle \cdot \langle \mathbf{Z} \rangle = 2U_0 = \boldsymbol{\Sigma}_0 \cdot \mathbf{Z}_0, \quad \langle \mathbf{Z} \rangle = \mathbf{Z}_0. \tag{9}$$

The averaged piezoelectric fields by volume Ω and by phase volumes Ω^r are determined by the formulas ($r = m, e, p$)

$$\langle \cdots \rangle = \frac{1}{|\Omega|} \int_\Omega (\cdots) d\Omega, \qquad \langle \cdots \rangle^r = \frac{1}{|\Omega|} \int_{\Omega^r} (\cdots) d\Omega. \tag{10}$$

As can be seen from (9), the energy relation is equivalent to the equality

$$\langle \boldsymbol{\Sigma} \rangle = \boldsymbol{\Sigma}_0. \tag{11}$$

Consequently, the homogenized properties (81 parameters) of the most generalized form of the piezoelectric composite can be determined by solving the homogenization problem with Eqs. (1)–(8), (10), (11) nine times using specific cases for the applied vector field $\mathbf{Z}_0$. So, to compute the effective moduli (8) in the column with number γ of the matrix $\boldsymbol{\Pi}^{\text{eff}}$, all external boundary conditions are set to zero except the component $\gamma = 1, 2, \ldots, 9$ of the vector $\mathbf{Z}_0$

$$Z_{0\beta} = Z_{0\gamma}\delta_{\beta\gamma} \Rightarrow \Pi_{\alpha\gamma}^{\text{eff}} = \langle \Sigma_\alpha \rangle / Z_{0\gamma}, \qquad \alpha, \beta = 1, 2, \ldots, 9. \tag{12}$$

Note that as has been proven,[30] the matrices of effective stiffnesses and permittivities must be symmetric, and the piezomoduli of the direct and converse piezoelectric effects must be equal: $c_{\alpha\beta}^{E\,\text{eff}} = c_{\beta\alpha}^{E\,\text{eff}}$, $\varepsilon_{ij}^{S\,\text{eff}} = \varepsilon_{ji}^{S\,\text{eff}}$, $e_{i\alpha}^{d\,\text{eff}} = e_{i\alpha}^{c\,\text{eff}} = e_{i\alpha}^{\text{eff}}$. This fact was also confirmed by numerical calculations for all considered composites.

In our study, nine ($\gamma = 1, 2, \ldots, 9$) homogenization problems with Eqs. (1)–(8), (10)–(12) for each variant of composite were solved using specialized algorithms and programs via ANSYS Mechanical APDL.

3. Results and Discussions

The conventional porous piezoelectric composites were extensively studied in many works,[12,35–38] and therefore we did not carry out a special study of the ordinary porous system (OPS). But in all subsequent figures, the effective moduli of the OPS and the system with a completely metalized pore surface (SCMPS) are provided, as reference cases, to reveal the influence of various cases of partially metalized pore surface on the effective material properties. We analyzed the relative values of the effective moduli, which are the ratios of the effective modulus value to the corresponding modulus of the dense piezoceramic material, for example, $r(c^E_{13}) = c^{E\text{eff}}_{13}/c^E_{13}$. In this way, the effective moduli of the composites are compared to the analogous moduli of the pure piezoelectric matrix. Our discussion focuses on the effective moduli of the systems with partially metalized pore surfaces (SPMPS). We studied four cases for the SPMPS. The SPMPS2X and the SPMPS2Z have two metalized pore sides; while, the SPMPS2X2Y and the SPMPS2X2Z have four metalized pore sides, as indicated earlier in Fig. 1.

3.1. *Exploring the effective moduli of the SPMPS2X and the SPMPS2Z*

The relative elastic modulus $r(c^E_{13})$ and the dielectric permittivity moduli $r(\varepsilon^S_{11})$ and $r(\varepsilon^S_{33})$ are shown in Figs. 2(a)–2(c), respectively, as functions of porosity. The effective elastic modulus $c^{E\text{eff}}_{13}$ reduces with the porosity growth, as seen in Fig. 2(a). Note that for all investigated piezocomposites, nonzero elastic moduli $c^{E\text{eff}}_{\alpha\beta}$ almost take the same trend of decrease with the porosity rise. Since the elastic moduli of the material filling the layer Ω^e are negligible, the pore surface metalization has a negligible effect on the effective elastic moduli. The dielectric moduli $r(\varepsilon^S_{11})$ and $r(\varepsilon^S_{33})$ of the SCMPS greatly increase with the porosity rise; however, the analogous moduli of the OPS decrease with the porosity growth. For example, at $\upsilon_c = 0.5$, the effective dielectric permittivity modulus $\varepsilon^{S\text{eff}}_{33}$ of the SCMPS increases about 1951% from the analogous modulus of the OPS. For the SPMPS2Z, as the porosity increases, the effective dielectric permittivity modulus $\varepsilon^{S\text{eff}}_{11}$ grows, but the effective dielectric permittivity modulus $\varepsilon^{S\text{eff}}_{33}$ reduces, as seen in Figs. 2(b) and 2(c). The dielectric permittivity moduli $\varepsilon^{S\text{eff}}_{11}$ and $\varepsilon^{S\text{eff}}_{33}$ of the SPMPS2X vary oppositely to those of the SPMPS2Z. In contrary to the pure piezoceramic PZT-5H, we observed that the dielectric permittivity moduli $\varepsilon^{S\text{eff}}_{11}$ and $\varepsilon^{S\text{eff}}_{22}$ of the SPMPS2X are not equal, as depicted in Fig. 2(b). This occurs due to the asymmetric construction of the metalized pore sides relative to the applied electric fields E_{01} and E_{02}, as discussed later.

Figure 3 presents the piezoelectric constants $r(e_{31})$, $r(e_{33})$, and $r(e_{15})$ versus porosity for the SPMPS2X and the SPMPS2Z. The effective piezomoduli e^{eff}_{33} and e^{eff}_{15} decrease with the porosity increase for all systems presented in Figs. 3(b) and 3(c). For the SPMPS2X, the effective piezomodulus e^{eff}_{33} decreases at a greater rate than the OPS; however, the effective piezomodulus e^{eff}_{15} is roughly identical to the OPS's analogous modulus with the porosity growth. For the SPMPS2Z, as the porosity grows, the effective piezomodulus e^{eff}_{33} nearly decreases like the OPS, but the effective shearing piezomodulus e^{eff}_{15} reduces at a slighter rate than the OPS. The main results in this discussion are those concerned with the relative piezoelectric modulus $r(e_{31})$ because it, unlike usual, increases in specific systems with increasing porosity. The transverse piezomodulus $|e^{\text{eff}}_{31}|$ of the SPMPS2X increases with the porosity growth, for $\upsilon_c \leq 0.2$, then slightly decreases with more porosity rise. However, the modulus $|e^{\text{eff}}_{31}|$ of the SPMPS2Z monotonically decreases when porosity increases, as shown in Fig. 3(a). For the SPMPS2X, $e^{\text{eff}}_{31} \neq e^{\text{eff}}_{32}$ and $e^{\text{eff}}_{24} \neq e^{\text{eff}}_{15}$, as shown in Figs. 3(a) and 3(c).

In Fig. 4, we plotted the system states related to the estimation of the effective piezomodulus e^{eff}_{31} and the effective

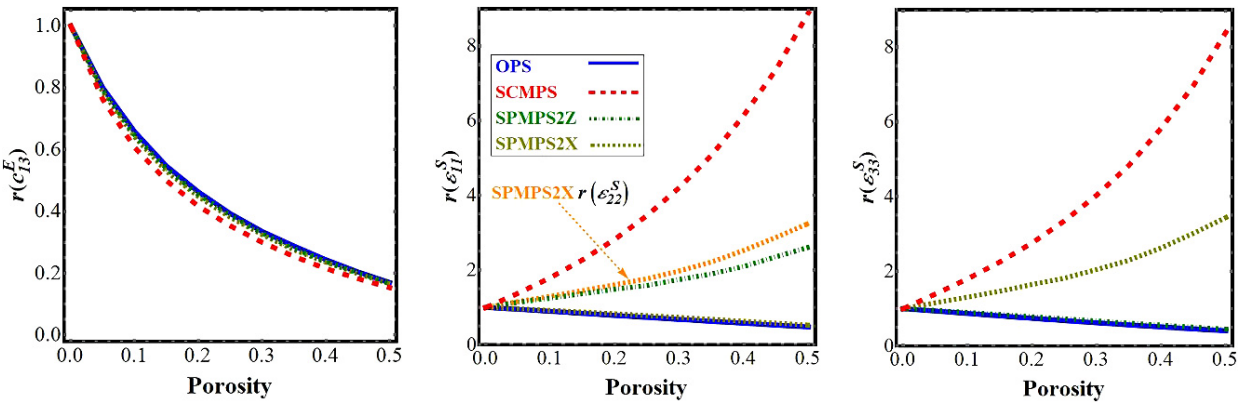

Fig. 2. The elastic modulus $r(c^E_{13})$ and the dielectric permittivity moduli $r(\varepsilon^S_{11})$ and $r(\varepsilon^S_{33})$ are plotted versus porosity in (a)–(c), respectively, for the systems SPMPS2X and SPMPS2Z.

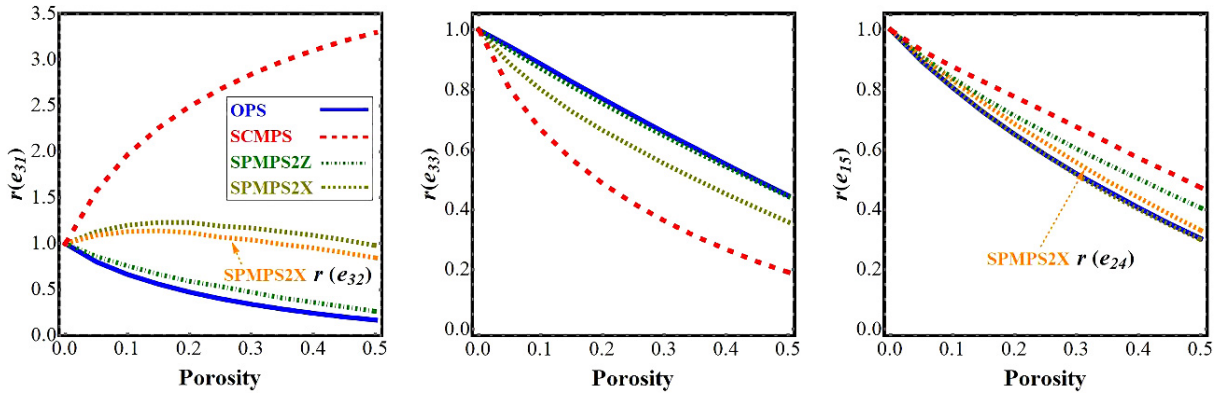

(a) (b) (c)

Fig. 3. The piezomoduli $r(e_{31})$, $r(e_{33})$, and $r(e_{15})$ are shown in (a)–(c), respectively, versus porosity for the systems SPMPS2X and SPMPS2Z.

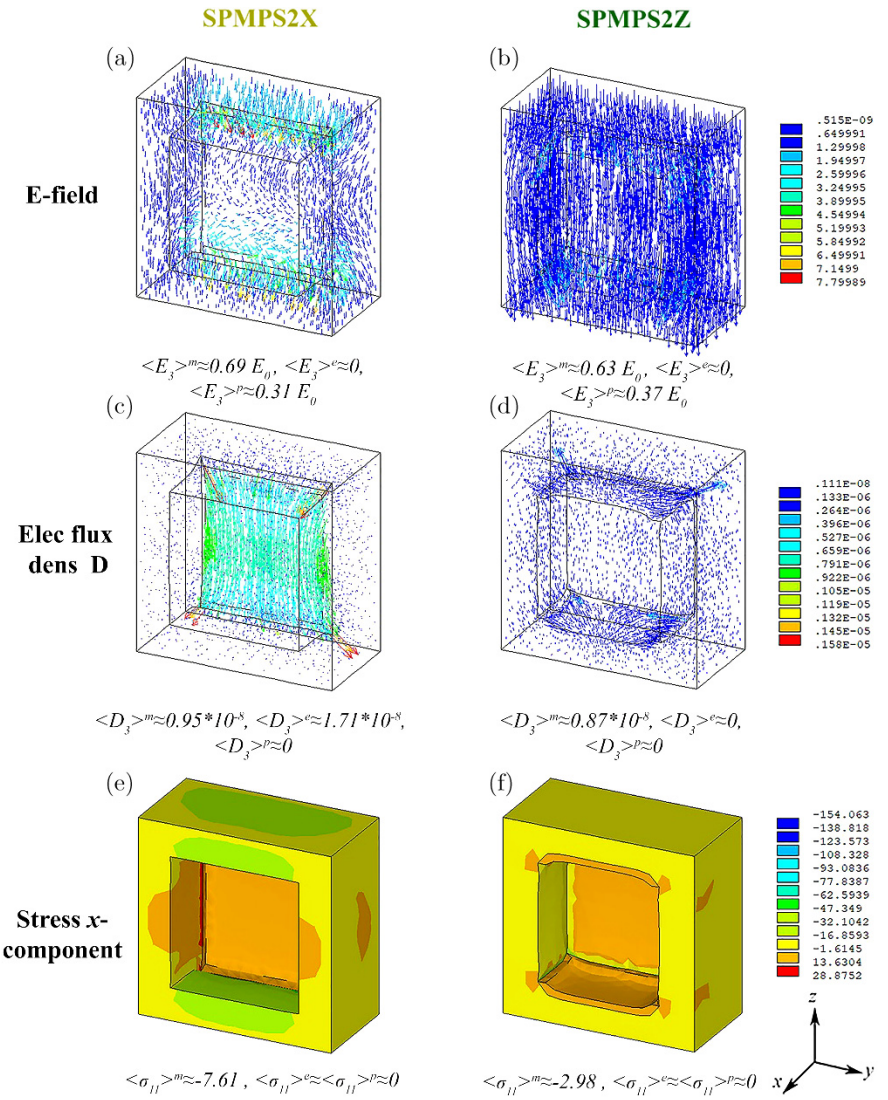

Fig. 4. The *E*-field vectors, the electric flux density vectors, and the strees *x*-component's contour plot are shown in (a), (c), and (e), respectively, for the SPMPS2X; and in (b), (d), and (f), respectively for the SPMPS2Z, in the half RVE without the vacuum pore at $\nu_c = 0.3$ with $E_{03} \neq 0$.

dielectric permittivity modulus $\varepsilon_{33}^{\text{Seff}}$. According to Eqs. (8), (10), and (12), the piezomodulus e_{31}^{eff} and the dielectric permittivity modulus $\varepsilon_{33}^{\text{Seff}}$ can be obtained using the boundary condition $E_{03} \neq 0$ as follows: $\varepsilon_{33}^{\text{Seff}} = \langle D_3 \rangle / \langle E_3 \rangle = (\langle D_3 \rangle^m + \langle D_3 \rangle^e + \langle D_3 \rangle^p)/E_{03}$ and $e_{31}^{\text{eff}} = \langle \sigma_{11} \rangle / E_{03} = (\langle \sigma_{11} \rangle^m + \langle \sigma_{11} \rangle^e + \langle \sigma_{11} \rangle^p)/E_{03}$. Since the vacuum dielectric permittivity is negligible, the integral value of the electric flux density generated in the pore volume ($\langle D_i \rangle^p$) tends to zero. So, the effective dielectric permittivity modulus $\varepsilon_{33}^{\text{Seff}}$ is proportional to the integral value $\langle D_3 \rangle^m + \langle D_3 \rangle^e$. The metalized pore sides can be considered as metal conductors placed in a region of a semi-regular electric field. The free charges of the conductor move freely to the polar regions, and the E-field within the conductor's volume vanishes. So, the conductor almost becomes a dipole. The metalized pore sides of the SPMPS2X create greater dipoles relative to those of the SPMPS2Z, owing to the geometric configurations of both systems. As a result, the integral values of the induced electric flux densities $\langle D_3 \rangle^m$ and $\langle D_3 \rangle^e$ are higher in the SPMPS2X than in the SPMPS2Z, as seen in Figs. 4(c) and 4(d). Which increases the SPMPS2X's effective dielectric permittivity modulus $\varepsilon_{33}^{\text{Seff}}$, as seen in Fig. 2(c).

When an E-field is externally applied in z-direction ($E_{03} \neq 0$), the mechanical stress generated in the compound pore Ω^c is negligible due to the minimal piezomoduli of the metal and vacuum phases. Consequently, the effective transverse piezomodulus e_{31}^{eff} depends on the integral value of stress generated in the piezoelectric phase ($\langle \sigma_{11} \rangle^m$). The presence of metalized pore sides causes dispersion in the electric field vectors, as seen in Figs. 4(a) and 4(b). Electric field vectors are more dispersed in the SPMPS2X than in the SPMPS2Z; because the SPMPS2X's metalized pore sides generate larger dipoles. This dispersion in the electric field vectors of the SPMPS2X raises the average values of stresses $\langle \sigma_{11} \rangle^m$ and $\langle \sigma_{22} \rangle^m$, as seen in Figs. 4(e) and 4(f); and decreases the average stresses $\langle \sigma_{33} \rangle^m$. Consequently, the effective transverse piezomodulus $|e_{31}^{\text{eff}}|$ of the SPMPS2X is higher than that of the SPMPS2Z. However, the longitudinal piezomodulus e_{33}^{eff} of the SPMPS2X is less than the SPMPS2Z, as shown in Figs. 3(a) and 3(b).

3.2. *Exploring the effective moduli of the SPMPS2X2Y and the SPMPS2X2Z*

Figure 5(a) presents the transverse elastic modulus $r(c_{13}^E)$ versus porosity. Due to the assumed negligible stiffness moduli of the metal layer, the elasticity coefficients of the SPMPS2X2Y and the SPMPS2X2Z are approximately equal to those of the SPMPS2X and the SPMPS2Z. The permittivity moduli $r(\varepsilon_{11}^S)$ and $r(\varepsilon_{33}^S)$ of the SPMPS2X2Z are nearly identical to those of the SCMPS. The permittivity modulus $r(\varepsilon_{11}^S)$ of the SPMPS2X2Y is almost identical to that of the SCMPS; whereas, the dielectric constant $r(\varepsilon_{33}^S)$ of the SPMPS2X2Y is smaller than the analogous modulus of the SCMPS, as seen in Figs. 5(b) and 5(c). Figure 5(b) indicates that the dielectric permittivity moduli $r(\varepsilon_{11}^S)$ and $r(\varepsilon_{22}^S)$ of the SPMPS2X2Z are not equal.

Figure 6 outlines that the piezomoduli of the SPMPS2X2Z are approximately identical to those of the SCMPS. The SPMPS2X2Y has greater longitudinal piezomodulus $r(e_{33})$ and smaller transverse piezomodulus $r(e_{31})$ and approximately identical shear piezomodulus $r(e_{15})$ compared to the SPMPS2X2Z, as observed clearly in Figs. 6(a)–6(c). For example, at $v_c = 0.3$, the effective piezomodulus $|e_{31}^{\text{eff}}|$ of the SCMPS, SPMPS2X2Z, and SPMPS2X2Y increases by 733%, 718%, and 378% from the corresponding modulus of the OPS. The change in piezoelectric and dielectric moduli in this way depends primarily on the structure of the metalized pore surface, as shown in the following discussion.

Figure 7 explains the system states associated with the piezoelectric modulus e_{31}^{eff} and the dielectric permittivity modulus $\varepsilon_{33}^{\text{Seff}}$ of the SPMPS2X2Y and the SPMPS2X2Z. These moduli

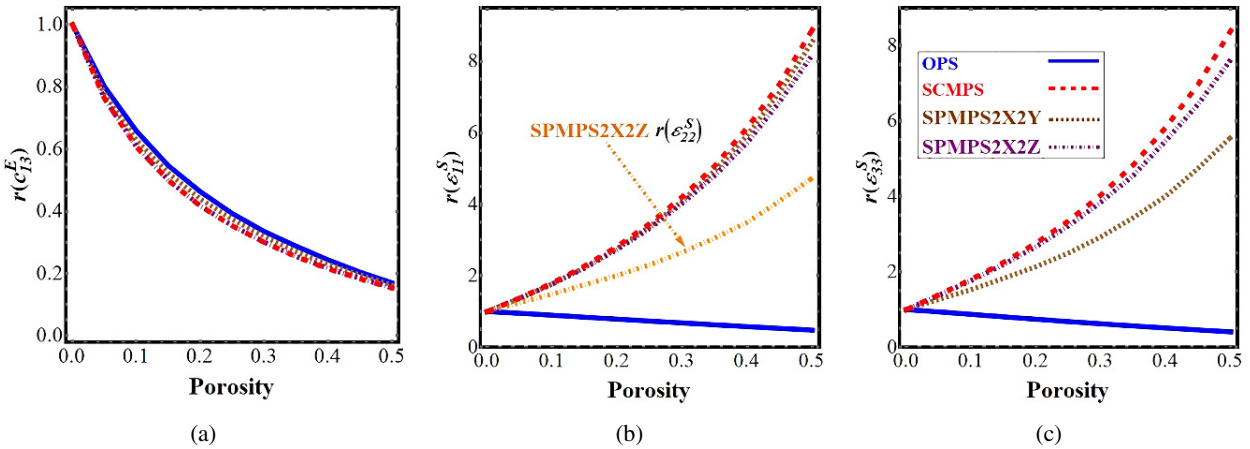

Fig. 5. (a) The relative elastic modulus $r(c_{13}^E)$, and the relative dielectric moduli $r(\varepsilon_{11}^S)$ and $r(\varepsilon_{33}^S)$ are shown in (a)–(c), respectively, versus porosity for the systems SPMPS2X2Y and SPMPS2X2Z.

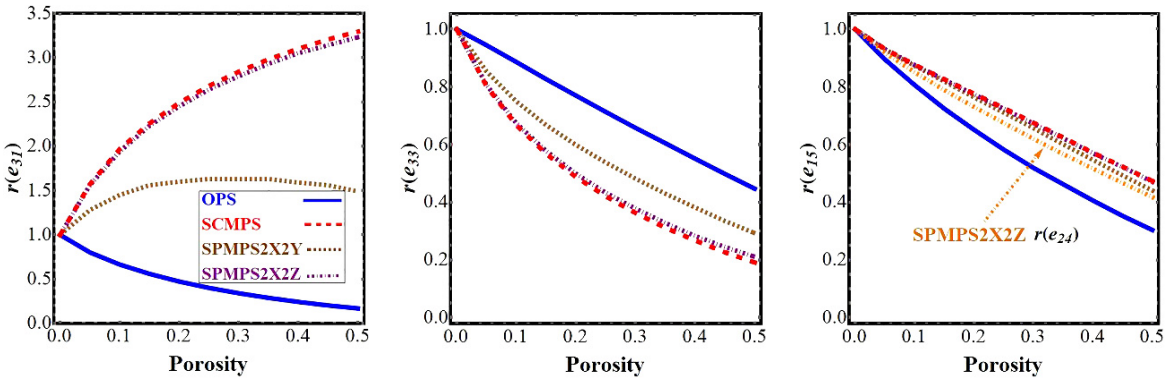

Fig. 6. The piezomoduli $r(e_3)$, $r(e_{33})$, and $r(e_{15})$ are shown in (a)–(c), respectively, versus porosity for the systems SPMPS2X2Y and SPMPS2X2Z.

can be explained in the same way as in the discussion of Fig. 4. The distribution of electric field vectors and electric flux density vectors in the SPMPS2X2Y and the SPMPS2X2Z can be clarified via Gauss's law as follows. If an electrical voltage is applied to both systems in z-direction ($E_{03} \neq 0$) such that the higher potential is on the top side, an electric field is produced, within the piezoelectric material, in the negative direction of the z-axis, as seen in Figs. 7(a) and 7(b).

For the SPMPS2X2Z, the metalized pore sides act as a closed conductor because the E-field vectors are perpendicular to the upper and lower metalized pore sides. The positive and negative charges move freely in the conductor generating an electric field E' inside the pore Ω^p, which opposes the original E-field ($E_{03} \neq 0$). The electric charges continue moving until vanishing the electric field inside the pore, i.e., $\langle E' \rangle$ approximately equals the integral value of the electric field inside the pore of the OPS $\langle E_3 \rangle^p$. The electric field outside the pore equals the sum $\langle E_3 \rangle^m + \langle E_3 \rangle^p$ in the corresponding OPS. According to this discussion, the applied electric field is optimally conserved within the volume of the piezoelectric phase ($\langle E_3 \rangle = \langle E_3 \rangle^m = E_{03}$).

The metalized pore sides of the SPMPS2X2Y do not form a closed surface w.r.t. the electric field applied in the direction z. The SPMPS2X2Y's metalized pore sides correspond just to a large dipole; they do not act as a closed cubic conductor w.r.t. the applied E-field ($E_{03} \neq 0$). So, the effective piezoelectric modulus $|e_{31}^{\text{eff}}|$ and dielectric permittivity modulus $\varepsilon_{33}^{S\text{eff}}$ of the SPMPS2X2Y are less extensive than those of the SPMPS2X2Z. For example, under the boundary condition $E_{03} \neq 0$ at $\upsilon_c = 0.3$, the SPMPS2X2Y preserves 76% of the electric field's effect in the piezoelectric volume Ω^m; however, the SPMPS2X2Z preserves 100% of the applied E-field within the piezoelectric volume under the same conditions, as shown in Figs. 7(a) and 7(b).

According to this discussion and Eqs. (8), (10), and (12), the obtained integral values $\langle D_3 \rangle^m$ and $\langle \sigma_{11} \rangle^m$ in the SPMPS2X2Z are greater than the corresponding values in the SPMPS2X2Y, as seen in Figs. 7(c)–7(f). Due to the greater absolute value of $\langle \sigma_{11} \rangle^m$, the effective piezomodulus $|e_{31}^{\text{eff}}|$ of the SPMPS2X2Z is more extensive than that of the SPMPS2X2Y, as Fig. 6(a) shows. Figures 7(c) and 7(d) show a higher interfacial polarization $\langle D_3 \rangle^e$ in the SPMPS2X2Z than in the SPMPS2X2Y. This phenomenon of increasing the dielectric permittivity moduli is due to the presence of a metal inclusion inside a dielectric medium.[39,40] Therefore, the SPMPS2X2Z's dielectric permittivity $\varepsilon_{33}^{S\text{eff}}$ is greater than that of the SPMPS2X2Y, as shown in Fig. 5(c). According to this discussion and Eqs. (8), (10), and (12), the SPMPS2X2Y keeps 100% of the applied E-fields for the cases $E_{01} \neq 0$ and $E_{02} \neq 0$ within the piezoelectric volume under the same conditions, thus the dielectric permittivities $\varepsilon_{11}^{S\text{eff}}$ and $\varepsilon_{22}^{S\text{eff}}$ of the SPMPS2X2Y are equal and higher than the dielectric permittivity modulus $\varepsilon_{22}^{S\text{eff}}$ of the SPMPS2X2Z, as shown in Fig. 5(b).

3.3. *Effects of the partially metalized pore surface on the crystal symmetry*

In the OPS and the SCMPS, the effective moduli with indices corresponding to Ox_1 axes and moduli with indices corresponding to Ox_2 axes are equal, i.e., $c_{11}^{E\text{eff}} = c_{22}^{E\text{eff}}$, $c_{13}^{E\text{eff}} = c_{23}^{E\text{eff}}$, $c_{44}^{E\text{eff}} = c_{55}^{E\text{eff}}$, $e_{31}^{\text{eff}} = e_{32}^{\text{eff}}$, $e_{24}^{\text{eff}} = e_{15}^{\text{eff}}$, $\varepsilon_{11}^{S\text{eff}} = \varepsilon_{22}^{S\text{eff}}$, and $c_{66}^{E\text{eff}} \approx (c_{11}^{E\text{eff}} - c_{12}^{E\text{eff}})/2$. So, the OPS and the SCMPS have the same hexagonal 6 mm crystal symmetry of the piezoceramic matrix PZT-5H. Owing to the configuration of the metalized pore faces, the SPMPS2X and SPMPS2X2Z do not fulfill this symmetry. These systems differently handle the electric field applied or induced in the x- and y-directions. For example, if the SPMPS2X2Z is subjected to the boundary conditions $E_{01} \neq 0$ and $E_{02} \neq 0$, the integral value $\langle D_1 \rangle$ will be higher than the integral value $\langle D_2 \rangle$, respectively; because the metalized pore sides in this system can be considered as a closed conductor only when the electric field is externally applied in x or z-directions. As a result, according to Eqs. (8), (10), and (12), the dielectric permittivity moduli $\varepsilon_{11}^{S\text{eff}}$ and $\varepsilon_{22}^{S\text{eff}}$ of the SPMPS2X2Z satisfy the relationship

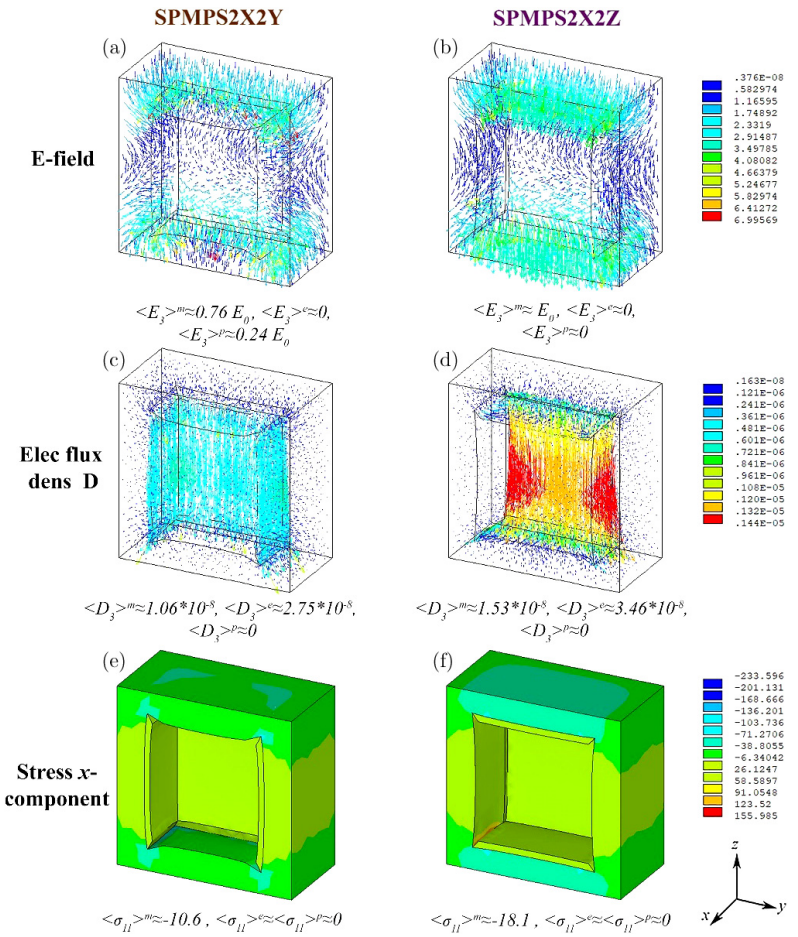

Fig. 7. The E-field vectors, the electric flux density vectors, and the stress x-component's contour plot are shown in (a), (c), and (e), respectively, for the SPMPS2X2Y; and in (b), (d), and (f), respectively, for the SPMPS2X2Z, in the half RVE without the vacuum pore at $\nu_c = 0.3$ with $E_{03} \neq 0$.

$\varepsilon_{11}^{S\text{eff}} > \varepsilon_{22}^{S\text{eff}}$. The crystal asymmetry can be well understood from the discussion of Figs. 4 and 7. This phenomenon was indicated in Figs. 2(b), 3(a), 3(c), 5(b), and 6(c). On contrary to the pure piezoceramics PZT-5H, the OPS, and the SCMPS, the SPMPS2X and the SPMPS2X2Z satisfy the crystal symmetry of mm2 orthorhombic systems.[41] For example, at $\upsilon_c = 0.3$, the effective electro-elastic properties $\mathbf{\Pi}^{\text{eff}}$ of the SPMPS2X have the following values:

$$\mathbf{\Pi}^{\text{eff}} = \left(\begin{array}{cccccc|ccc} 5.751\cdot10^{10} & 2.772\cdot10^{10} & 2.718\cdot10^{10} & 0 & 0 & 0 & 0 & 0 & 7.61 \\ 2.772\cdot10^{10} & 5.805\cdot10^{10} & 2.732\cdot10^{10} & 0 & 0 & 0 & 0 & 0 & 6.77 \\ 2.718\cdot10^{10} & 2.732\cdot10^{10} & 4.778\cdot10^{10} & 0 & 0 & 0 & 0 & 0 & -12.9 \\ 0 & 0 & 0 & 1.254\cdot10^{10} & 0 & 0 & 0 & -9.4 & 0 \\ 0 & 0 & 0 & 0 & 1.251\cdot10^{10} & 0 & -8.74 & 0 & 0 \\ 0 & 0 & 0 & 0 & 0 & 1.246\cdot10^{10} & 0 & 0 & 0 \\ \hline 0 & 0 & 0 & 0 & 8.74 & 0 & 1.1\cdot10^{-8} & 0 & 0 \\ 0 & 0 & 0 & 9.4 & 0 & 0 & 0 & 2.98\cdot10^{-8} & 0 \\ -7.61 & -6.77 & 12.9 & 0 & 0 & 0 & 0 & 0 & 2.66\cdot10^{-8} \end{array}\right).$$

In the previous matrix, it can be shown that applying metallization perpendicular to only one axis Ox_1 leads to a very large difference between the effective dielectric permittivity moduli $\varepsilon_{11}^{S\text{eff}}$ and $\varepsilon_{22}^{S\text{eff}}$ and to a rather significant difference between the effective piezomoduli e_{31}^{eff} and e_{32}^{eff}, and the effective piezomoduli e_{15}^{eff} and e_{24}^{eff}.

Since here, the metalized pore sides are assumed to have negligible elastic properties, the change in crystal symmetry slightly appears in the elastic moduli, but nonetheless $c_{11}^{E\,\text{eff}} \neq c_{22}^{E\,\text{eff}}$, $c_{13}^{E\,\text{eff}} \neq c_{23}^{E\,\text{eff}}$, and $c_{44}^{E\,\text{eff}} \neq c_{55}^{E\,\text{eff}}$, and $c_{66}^{E\,\text{eff}} \neq (c_{11}^{E\,\text{eff}} - c_{12}^{E\,\text{eff}})/2$. This change in crystal symmetry

regarding the elastic properties is due to the influence of the piezoelectric effect on the elastic properties.

4. Conclusions

This paper investigates a porous piezocomposite consisting of a ceramic matrix with superlattices of closed pores coated with metal particles. At the interface surface between the piezoceramic phase and the void, these particles produce a metal coating with negligible thickness. We considered a simple representative volume consisting of a cubic piezoceramic matrix and containing at its center a cubic compound pore consisting of a vacuum pore and coated with a metal sheet of a minimal thickness. Because of the possible deficiencies in the metalization process, the porous piezocomposite with a completely metalized pore surface is challenging to be physically constructed. Consequently, the homogenized properties of porous piezocomposites with a partly metalized pore surface have been discussed here. Different metalization processes are simulated by analyzing the effective moduli of porous piezocomposites with four and two metalized pore sides, respectively. We found that the effective moduli of the systems with four metalized pore sides, in which the metal layer coats 67% (four sides) of the pore surface, are almost near to those of the system with a completely metalized pore surface. The dielectric permittivity moduli of structures with sufficiently metalized pore surfaces increase monotonically as porosity increases. This enhancement of effective permittivity moduli is due to the interfacial polarization induced by the excessive electric field at the limiting neighborhood of the interface between the piezoelectric and metal phases. The absolute value of the transverse piezomodulus of a sufficiently metalized porous piezocomposite significantly increases with the growth of porosity; since the presence of the metal layer induces dispersion in the electric field vectors and preserves their influence in the piezoelectric phase. In the piezocomposites with partially metalized pore surfaces, the following asymmetries were observed due to the dependence of piezoelectric and dielectric permittivity moduli on the configuration of the metalized pore sides: $e_{31}^{\text{eff}} \neq e_{32}^{\text{eff}}$, $e_{24}^{\text{eff}} \neq e_{15}^{\text{eff}}$, $\varepsilon_{11}^{S\text{eff}} \neq \varepsilon_{22}^{S\text{eff}}$, $c_{11}^{E\text{eff}} \neq c_{22}^{E\text{eff}}$, $c_{13}^{E\text{eff}} \neq c_{23}^{E\text{eff}}$, $c_{44}^{E\text{eff}} \neq c_{55}^{E\text{eff}}$, and $c_{66}^{E\text{eff}} \neq (c_{11}^{E\text{eff}} - c_{12}^{E\text{eff}})/2$. These asymmetries are predicted to occur with more complex representative volumes that contain many closed pores with randomly metalized pore surfaces. The piezocomposites with partially metalized pore surfaces may have higher anisotropy (orthorhombic mm2 system) compared to lower anisotropy of the piezoceramic matrix (hexagonal 6 mm system). Further we intend to study the homogenization problem presented here using such complicated representative volumes.

Acknowledgments

This research was done in the framework of the RFBR project 20-31-90102.

References

[1]K. K. Shung, J. M. Cannata and Q. F. Zhou, Piezoelectric materials for high frequency medical imaging applications: A review, *J. Electroceramics* **19**, 139 (2007).
[2]M. S. Vijaya, *Piezoelectric Materials and Devices: Applications in Engineering and Medical Sciences* (CRC Press, Boca Raton, 2012).
[3]H. Elahi *et al.*, A review on applications of piezoelectric materials in aerospace industry, *Integr. Ferroelectr.* **211**, 25 (2020).
[4]J. A. B. Gripp and D. A. Rade, Vibration and noise control using shunted piezoelectric transducers: A review, *Mech. Syst. Signal Process* **112**, 359 (2018).
[5]L.-P. Wang *et al.*, Design, fabrication, and measurement of high-sensitivity piezoelectric microelectromechanical systems accelerometers, *J. Microelectromech. Syst.* **12**, 433 (2003).
[6]J. M. W. Brownjohn, Structural health monitoring of civil infrastructure, *Phil. Trans. R. Soc. A* **365**, 589 (2007).
[7]S. Geis, P. Löbmann, S. Seifert and J. Fricke, Dielectric properties of PZT aerogels, *Ferroelectrics* **241**, 75 (2000).
[8]W. A. Smith, The role of piezocomposites in ultrasonic transducers, in *Proc. IEEE Ultrasonics Symp.* (Montreal, QC, Canada, 1989), Vol. 2, pp. 755–766.
[9]C. N. Della and D. Shu, The performance of 1–3 piezoelectric composites with a porous non-piezoelectric matrix, *Acta Mater.* **56**, 754 (2008).
[10]K. Hikita, K. Yamada, M. Nishioka and M. Ono, Piezoelectric properties of the porous PZT and the porous PZT composite with silicone rubber, *Ferroelectrics* **49**, 265 (1983).
[11]U. Bast and W. Wersing, The influence of internal voids with 3–1 connectivity on the properties of piezoelectric ceramics prepared by a new planar process, *Ferroelectrics* **94**, 229 (1989).
[12]C. R. Bowen, A. Perry, A. C. F. Lewis and H. Kara, Processing and properties of porous piezoelectric materials with high hydrostatic figures of merit, *J. Eur. Ceram. Soc.* **24**, 541 (2004).
[13]K. Mehta and A. V. Virkar, Fracture mechanisms in ferroelectric-ferroelastic lead zirconate titanate (Zr: Ti= 0.54: 0.46) ceramics, *J. Am. Ceram. Soc.* **73**, 567 (1990).
[14]S.-J. Yoon, J. H. Moon and H.-J. Kim, Piezoelectric and mechanical properties of Pb (Zr 0.52 Ti 0.48) O 3–Pb (Y 2/3 W 1/3) O 3 (PZT–PYW) ceramics, *J. Mater. Sci.* **32**, 779 (1997).
[15]W. Liu, N. Li, Y. Wang, H. Xu, J. Wang and J. Yang, Preparation and properties of 3–1 type PZT ceramics by a self-organization method, *J. Eur. Ceram. Soc.* **35**, 3467 (2015).
[16]P.-H. Xiang, X.-L. Dong, H. Chen, Z. Zhang and J.-K. Guo, Mechanical and electrical properties of small amount of oxides reinforced PZT ceramics, *Ceram. Int.* **29**, 499 (2003).
[17]T. Xu and C.-A. Wang, Piezoelectric properties of a pioneering 3-1 type PZT/epoxy composites based on freeze-casting processing, *J. Am. Ceram. Soc.* **97**, 1511 (2014).
[18]H. L. Zhang, J. F. Li and B. P. Zhang, Fabrication and evaluation of PZT/Ag composites and functionally graded piezoelectric actuator, *J. Electroceram.* **16**, 413 (2006).
[19]K. Takagi, J.-F. Li, S. Yokoyama and R. Watanabe, Fabrication and evaluation of PZT/Pt piezoelectric composites and functionally graded actuators, *J. Eur. Ceram. Soc.* **23**, 1577 (2003).
[20]J. Li *et al.*, Fabrication and evaluation of porous piezoelectric ceramics and porosity–graded piezoelectric actuators, *J. Am. Ceram. Soc.* **86**, 1094 (2003).

[21]K. Horikiri, T. Yanaseko, I. Kuboki, H. Sato and H. Asanuma, Development of surface oxidized metal fiber/piezoelectric ceramics/aluminum composite, *Mech. Eng. J.* **6**, 18-00556 (2019).
[22]T. Yanaseko, H. Asanuma and H. Sato, Characterization of a metal-core piezoelectric ceramics fiber/aluminum composite, *Mech. Eng. J.* **14**, 14-00357 (2015).
[23]T. Yanaseko, I. Kuboki, H. Sato and H. Asanuma, Investigation of fabrication condition of metal matrix piezoelectric composite using surface oxidized metal fiber as internal electrode, *Proc. Int. Conf. Leading Edge Manufacturing/Materials and Processing, LEMP2020*, 8576 (2021).
[24]A. N. Rybyanets and A. A. Naumenko, Nanoparticles transport in ceramic matries: A novel approach for ceramic matrix composites fabrication, *J. Mod. Phys.* **4**, 1041 (2013).
[25]A. N. Rybyanets, I. A. Shvetsov, M. A. Lugovaya, E. I. Petrova and N. A. Shvetsova, Nanoparticles transport using polymeric nano- and microgranules: Novel approach for advanced material design and medical applications, *J. Nano-Electron. Phys.* **10**, 02005 (2018).
[26]A. Nasedkin and M. E. Nassar, Effective properties of a porous inhomogeneously polarized by direction piezoceramic material with full metalized pore boundaries: Finite element analysis, *J. Adv. Dielectr.* **10**, 2050018 (2020).
[27]R. E. Newnham, D. P. Skinner and L. E. Cross, Connectivity and piezoelectric-pyroelectric composites, *Mater. Res. Bull.* **13**, 525 (1978).
[28]G. Martínez-Ayuso, M. I. Friswell, S. Adhikari, H. H. Khodaparast and H. Berger, Homogenization of porous piezoelectric materials, *Int. J. Solids Struct.* **113–114**, 218 (2017).
[29]H. Berger *et al.*, An analytical and numerical approach for calculating effective material coefficients of piezoelectric fiber composites, *Int. J. Solids Struct.* **42**, 5692 (2005).
[30]A. V. Nasedkin, A. A. Nasedkina and M. E. Nassar, Homogenization of porous piezocomposites with extreme properties at pore boundaries by effective moduli method, *Mech. Solids* **55**, 827 (2020).
[31]A. V. Nasedkin and M. S. Shevtsova, Improved finite element approaches for modeling of porous piezocomposite materials with different connectivity, in *Ferroelectrics and Superconductors: Properties and Applications*, ed. I. A. Parinov, Chap. 7 (Nova Science Publishers, New York, 2011), pp. 231–254.
[32]A. V. Nasedkin and M. S. Shevtsova, Multiscale computer simulation of piezoelectric devices with elements from porous piezoceramics, in *Physics and Mechanics of new Materials and their Applications*, Chap. 16, eds. I. A. Parinov and S.-H. Chang (Nova Science Publishers, New York, 2013), pp. 185–202.
[33]M. Hori and S. Nemat-Nasser, Universal bounds for effective piezoelectric moduli, *Mech. Mater.* **30**, 1 (1998).
[34]J. Aboudi, *Mechanics of Composite Materials: A Unified Micromechanical Approach* (Elsevier, Amsterdam, 2013).
[35]M. L. Dunn and M. Taya, Electromechanical properties of porous piezoelectric ceramics, *J. Am. Ceram. Soc.* **76**, 1697 (1993).
[36]S. Iyer and T. A. Venkatesh, Electromechanical response of porous piezoelectric materials: Effects of porosity connectivity, *Appl. Phys. Lett.* **97**, 072904 (2010).
[37]S. Iyer and T. A. Venkatesh, Electromechanical response of (3-0) porous piezoelectric materials: Effects of porosity shape, *J. Appl. Phys.* **110**, 034109 (2011).
[38]S. Iyer and T. A. Venkatesh, Electromechanical response of (3–0, 3–1) particulate, fibrous, and porous piezoelectric composites with anisotropic constituents: A model based on the homogenization method, *Int. J. Solids Struct.* **51**, 1221 (2014).
[39]H. Du, X. Lin, H. Zheng, B. Qu, Y. Huang and D. Chu, Colossal permittivity in percolative ceramic/metal dielectric composites, *J. Alloys Compd.* **663**, 848 (2016).
[40]J. I. Roscow, C. R. Bowen and D. P. Almond, Breakdown in the case for materials with giant permittivity?, *ACS Energy Lett.* **2**, 2264 (2017).
[41]ANSI/IEEE Std, 176–1987. *IEEE Standard on Piezoelectricity* (IEEE, New York, 1987).